

DAMAGE MECHANICS MODELING OF CONCURRENT THERMAL AND VIBRATION LOADING ON ELECTRONICS PACKAGING

Juan Gomez¹, Minghui Lin¹ and Cemal Basaran^{*2}

¹Research Assistant, UB Electronic Packaging Laboratory.

²Professor, and Director, UB Electronic Packaging Laboratory University at Buffalo, State University of New York

Received 3 February 2005; accepted 26 October 2005

Abstract— The problem of concurrent thermal and vibration loading has not been thoroughly studied even though it is common in electronic packaging applications. Here we attempt to address such a problem using a damage mechanics based constitutive model. Damage mechanics constitutive model for eutectic Pb/Sn solder alloys is used to simulate the damage effects of concurrent cyclic thermal loads and vibrations on Ball Grid Array (BGA) packages. The model is implemented into the commercial finite element code ABAQUS through its user defined material subroutine capability. For the integration algorithm we have used a return mapping scheme, which dramatically improves the convergence rate as compared to previous implementations of the same model. Results are examined in terms of accumulation of plastic strain within the solder connections. It is shown that the simplistic Miner's rule can not accurately account for the combined effect of both loadings acting concurrently.

Keywords: Finite element analysis, constitutive model, dynamic analysis, concurrent loading, microelectronics packaging, solder joints.

1. INTRODUCTION

The most common mode of failure in microelectronic packaging solder joints is low cycle fatigue. Temperature changes and the coefficient of thermal expansion mismatch between the soldered parts is the main reason behind the fatigue. When an electronic package undergoes a temperature variation interconnects are stressed mainly in cyclic shear. The stresses impart elastic and inelastic strains, which are also cyclic in nature leading to thermo mechanical fatigue. The temperatures changes are due to switch on/off operations or sometimes owing to fluctuations in the ambient conditions. On the other hand, eutectic solder alloys are routinely used at high homologous temperatures. The melting point of the eutectic Sn/Pb solder alloy is 183°C, and it is at 0.65T_m at room temperature, where T_m is the melting point. Therefore, solder joints exhibit time, temperature, stress dependent deformation behavior and such coupling makes constitutive modeling a difficult task. Material models ranging from purely elastic to elasto-visco-plastic using various stress-strain relations have been proposed for Sn/Pb

* E-mail: cjb@buffalo.edu

solder alloys, such as in Kitano et al.(1988),[1], Lau & Rice(1990),[2], Basaran et al.(1998),[3] and many others. Adams (1986), [4] proposed a simple viscoplastic model without hardening. Wilcox et al (1989), [5], proposed a rheological model to represent the inelastic behavior of the material, however it is applicable to a limited range of strain rates. The purely phenomenological models proposed by Knoch and Fox (1990), [6], Darveaux and Banerji (1992), [7] and Hong and Burrell (1995), [8] decoupled the creep and plasticity effects artificially. This decoupling does not have any physical basis and is just motivated by mathematical convenience. Classical forms of decoupled plasticity and creep theories have been shown to be quite inferior for modeling cyclic plasticity, creep and interaction effects, Mcdowell et al(1994),[9]. Recently, Zhao(2000),[10], followed by Basaran and Tang (2002), [11] and Tang (2002), [12] have extended a creep law originally proposed by Kashyap and Murty(1998), [13] for eutectic solder alloys into a thermodynamics based framework for low cycle fatigue predictions. The model has been validated against thermomechanical fatigue experiments, Gomez and Basaran, (2005a), [14], performed on thin layer solder joints and nanoindentation experiments at room temperature, Gomez and Basaran (2005b), [15]. Another source of failure in electronic equipment is vibrations, Steinberg (2000), [16]. It is common for electronic equipment to be subjected to vibrations over a wide range of frequencies and acceleration levels. For instance, according to the US Air Force, vibration and shock loads are responsible for the mechanical failure of 20 percent of airborne electronics. These vibrations may occur simultaneously with thermal loads at some time during the service life of the structure. However, this combined effect has not been thoroughly studied or understood by the electronic packaging community, Basaran et al (2001), [17]. This is in part because of the lack of robust constitutive models to predict the creep-vibration-fatigue interaction effects on eutectic solder alloys. Also the vibration and thermal cycling effects occur at different time scales which make the computational treatment highly expensive. On the other hand, there is not enough experimental data for verification of the computational models. In this paper we have implemented a constitutive model into the commercial finite element code ABAQUS through its user defined material subroutine capabilities. We have used a return mapping scheme as proposed in Simo and Hughes (1997), [18]. Previous ABAQUS implementations of similar models like in Tang(2002), [12], Basaran and Tang (2002), [11], Basaran et al(2005),[17] have made use of the Owen and Hinton(1980),[19] viscoplasticity integration scheme which when ported into ABAQUS exhibits very low convergence rate making it impractical if not impossible for dynamic loading applications. The main goal of the present paper is to study the combined effect of dynamic loads applied concurrently with thermal cycling. Although we do not directly calculate the fatigue life in our simulations, conclusions about the fatigue life are inferred from the computed inelastic strains and damage parameter under combined conditions. Experimentally, this problem was addressed by Zhao et al (1999), [20] where concurrent vibration and thermal cycling was performed on a commercial electronic package using a dynamic shaker embedded into a controlled thermal chamber. The effect on fatigue life of the concurrent loading conditions was described in terms of the plastic strains measured by high sensitivity Moire interferometer technique. Based on the boundary conditions, and loading profile they used it was concluded that the fatigue life is improved when the loads are applied concurrently and that the commonly used Miner's rule to superimpose the effects of the two loads acting independently is inaccurate. According to Barker et al (1990), [21],

Miner's rule, Miner (1945), [22] assumes that every structural member has a useful fatigue life and that every stress cycle uses up a part of this life. Furthermore, if the strains from vibrational and thermal loading are available, Miner's rule assumes that the

fatigue life can be characterized like $R = \frac{n_{th}}{N_{th}} + \frac{n_v}{N_v}$ where R is the ratio of number of

cycles experienced n_i to the fatigue life N_i at a specific i^{th} strain level. The fatigue life at a given strain level is commonly computed using Coffin-Manson relations or modified Coffin-Manson relations which was developed for structural steel. Miner's rule is intended as a first order approximation since it can not account for factors like creep and the temperature dependent dynamic properties of the structure. For instance, as the thermal load progresses certain parts of the package may soften or harden, leading also to changes in the "natural" frequencies of the structure and therefore to its dynamic response. However, we inhere show that even if the superposition trend of the Miner's rule is correct, it may not yield accurate results quantitatively when predicting fatigue life because it does not account for nonlinearities that may occur during the loading process. Moreover, we show here that Miner's rule may lead to non-conservative results. In order to prove our point we have conducted two sets of finite element analysis. First, we model a commercial personal computer PCB with all the mounted components where we conduct several analyses to show that the trend behind Miners rule is correct. Then we model a microprocessor package where we conduct several analyses to show that the trend behind Miner's rule is correct qualitatively. In this work we assume that the equivalent plastic strain reveals the damage trend even if it may not be quantitatively very accurate, Basaran et al (2005), [17].

2. MATERIAL CONSTITUTIVE MODEL

In the implemented constitutive model the return mapping scheme is the one after Simo and Hughes (1998), [18] and Lubarda and Benson (2002), [23] viscoplastic integration and the Alfano et al (2001), [24] scheme for the nonlinear kinematic hardening model are used. Damage is introduced using the effective stress concept and the strain equivalence principle. Rate dependent effects are considered by means of the viscous overstress concept. Here we present the flow theory formulation following the classical approach in terms of a yield function separating the elastic from the viscoplastic domain, a flow rule specifying the evolution of the viscoplastic strain, a set of hardening laws specifying the evolution of the hardening parameters and the evolution of damage like an additional state variable. In order to describe the model it is convenient to first present the equations for a rate independent material without any damage.

2.1. Hooke's Law

For a classical Von Mises rate independent plasticity model with isotropic behavior Hooke's law reads

$$\dot{\sigma} = C : (\dot{\epsilon} - \dot{\epsilon}^p - \dot{\epsilon}^\theta) \quad (1)$$

where $\dot{\epsilon}$, $\dot{\epsilon}^p$ and $\dot{\epsilon}^\theta$ are the rates of total strain, plastic strain and thermal strain respectively, C is the elastic constitutive tensor and $:$ represents contraction between two tensors.

2.2. Yield surface

The elasto-plastic domain is defined according to the following yield function

$$F = \|S - X\| - \sqrt{\frac{2}{3}}K(\alpha) \equiv \|S - X\| - R(\alpha) \quad (2)$$

where $F(\sigma, \alpha)$ is a yield surface separating the elastic from the inelastic domain, X is the deviatoric component of the back stress describing the position of the center of the yield surface in stress space, S is the deviatoric component of the stress tensor, $\|A\| \equiv \sqrt{A \cdot A}$ represents the norm of a given tensor A , $R(\alpha) \equiv \sqrt{\frac{2}{3}}K(\alpha)$ describes the radius of the yield surface in stress space.

2.3. Flow rule

The evolution of the plastic strain is represented by the general flow rule,

$$\dot{\epsilon}^p = \gamma \hat{n} \quad (3)$$

with $\hat{n} = \frac{\partial F}{\partial \sigma}$ being the normal to the yield surface.

2.4. Isotropic hardening

Isotropic hardening is described by the evolution of the radius of the yield surface according to

$$K(\alpha) = \sqrt{\frac{2}{3}}Y_0 + R_\infty (1 - e^{-c\alpha}) \quad (4a)$$

where α is a plastic consistency parameter or plastic strain trajectory evolving according to (4b), Y_0 is the initial yield stress, R_∞ is an isotropic hardening saturation value and c is an isotropic hardening rate.

$$\dot{\alpha} = \sqrt{\frac{2}{3}}\gamma \quad (4b)$$

2.5. The Non-Linear-Kinematic Hardening (NLK) Rule

The NLK rule is taken from Chaboche (1989), [25] and was originally proposed by Armstrong and Frederic (1966),[26]. Non-linearities are introduced as a recall term to the Prager (1956), [27] linear rule.

$$\dot{X} = c_1 \dot{\epsilon}^p - c_2 X \dot{\alpha} \quad (5)$$

The first term represents the linear kinematic hardening as defined by Prager. The second term is a recall term, often called a dynamic recovery term, which introduces the non-linearity between the back stress X and the actual plastic strain. When $c_2 = 0$ Eqn. (5) reduces to the linear kinematic rule. The NLK equation describes the rapid changes due to the plastic flow during cyclic loadings and plays an important role even under stabilized conditions (after saturation of cyclic hardening). In other words, these equations take into account the transient hardening effects in each stress-strain loop. After unloading, dislocation remobilization is implicitly described due to the back stress effect and the larger plastic modulus at the beginning of the reverse plastic flow Chaboche (1989), [25]. Note than in equation (5) c_1 corresponds to the term $\frac{2}{3}C$ in the original formulation and described in Basaran et al (2005), [17].

In the equations above, γ is a non-negative plasticity (consistency) parameter representing the irreversible character of plastic flow and obeying the following properties.

1. For a rate independent material model γ obeys the so-called loading/unloading and consistency condition

$$\gamma \geq 0 \text{ and } F(\sigma, \alpha) \leq 0 \tag{6}$$

$$\gamma \dot{F}(\sigma, \alpha) = 0 \tag{7}$$

2. For a rate dependent material model conditions (6) and (7) are replaced by a constitutive equation of the form.

$$\gamma = \frac{\langle \phi(F) \rangle}{\eta} \tag{8}$$

where η represents a viscosity material parameter.

In the case of a rate independent material F satisfies conditions (6) and (7) and additionally stress states such $F(\sigma, \alpha) > 0$ are ruled out. In the case of a rate dependent material on the other hand, the magnitude of the viscoplastic flow is proportional to the distance of the stress state to the surface defined by $F(\sigma, \alpha) = 0$. Using this fact we have after using Eqn.(8) that the following relation can be established

$$F = \Theta(\gamma\eta) \tag{9}$$

where $\Theta(\gamma\eta) = \phi^{-1}(\gamma\eta)$.

2.6. Viscoplastic creep law

In this particular model the creep law is the one proposed by Kashyap and Murty (1981), [12] and extended to multiaxial case by Basaran and Tang (2002), [11] and given by

$$\dot{\epsilon}_{ij}^{vp} = \frac{AD_0Eb}{k\theta} \left(\frac{\langle F \rangle}{E} \right)^n \left(\frac{b}{d} \right)^p e^{-Q/R\theta} \frac{\partial F}{\partial \sigma_{ij}} \tag{10}$$

where, A is a dimensionless material parameter which is temperature and rate dependent,

$D_i = D_0 e^{-Q/R\theta}$ is a diffusion coefficient with D_0 representing a frequency factor, Q is the creep activation energy, R is the universal gas constant, θ is the absolute temperature in Kelvin, $E(\theta)$ is a temperature dependent Young's modulus, b is the characteristic length of crystal dislocation (magnitude of Burger's vector), k is Boltzman's constant, d is the average grain size, p is a grain size exponent, n is a stress exponent for plastic deformation rate, where $1/n$ indicates strain sensitivity.

From Eqn.(10) we can identify $\langle \phi(F) \rangle = \langle F \rangle^n$ and $\eta = \frac{k\theta}{AD_0 E^{n-1} b} \left(\frac{d}{b}\right)^p e^{Q/R\theta}$.

2.7. Damage coupled elasto-viscoplastic model

Making use of the strain equivalence principle we can write in the usual form, Lemaitre (1996), [28]

$$\dot{\sigma} = (1-D)C : (\dot{\epsilon} - \dot{\epsilon}^{vp} - \dot{\epsilon}^\theta) \quad (11)$$

$$F = \|S - X^D\| - (1-D) \sqrt{\frac{2}{3}} K(\alpha) \equiv \|S - X^D\| - (1-D) R(\alpha) \quad (12)$$

where D is a damage metric and

$$\dot{X}^D = (1-D)(c_1 \dot{\epsilon}^{vp} - c_2 X \dot{\alpha}) \quad (13)$$

2.8. Formulation of damage function

Damage is considered following the approach by Basaran and Yan (1998), [29], Tang (2002), [12], Basaran and Nie (2004), [30], where the relation between the disorder and entropy established by Boltzmann using statistical mechanics and the second law of thermodynamics is exploited. Their thermodynamic framework assumes that damage and the disorder are analogous concepts and the thermodynamic disorder can be used to model the damage evolution. The damage formulation used here has the advantage over other damage formulations that is not derived from a damage potential and therefore there are not additional material properties. Thus, damage can be completely characterized using standard material properties. The Damage evolution function is given by

$$D = \left(1 - e^{-((\Delta e - \Delta \phi)/(N_0 k \theta / \bar{m}_s))} \right) D_{cr} \quad (14)$$

where

D_{cr} is a damage threshold

$\Delta e - \Delta \phi$ is the difference between the changes in the internal energy and the Helmholtz free energy with respect to a reference state. This difference is obtained as follows: the internal energy equation, which is an expression of the first law of thermodynamics, reads

$$\rho \frac{de}{dt} = \sigma_{ij} D_{ij}^m + \rho \hat{\gamma} - q_{i,i} \quad (15)$$

where D_{ij}^{in} is the rate of deformation tensor. For the particular case of small strains and small displacements $D_{ij}^{in} = \frac{d\varepsilon_{ij}^{in}}{dt}$. $\hat{\gamma}$ is the internal heat production rate and q_i is the rate of heat flux through the surface. The Helmholtz free energy is written in terms of the stress tensor thus

$$\rho \frac{d\psi}{dt} = \sigma_{ij} D_{ij}^{in} \quad (16)$$

After combining Eqs. (15) and (16), the difference between the changes in the internal energy and the Helmholtz free energy with respect to a reference state is obtained as follows;

$$\Delta e - \Delta \phi = \frac{1}{\rho} \int_{t_1}^{t_2} \sigma_{ij}^S D_{ij}^{in} dt + \int_{t_1}^{t_2} \gamma dt - \int_{t_1}^{t_2} q_{i,i} dt \quad (17)$$

This damage evolution model and integration algorithm has been verified against nanoindentation and fatigue experiments performed at the UB electronic packaging lab under different temperatures and imposed displacement rate conditions, Basaran and Yan (1998), [29], Basaran and Tang (2002), [11], Gomez and Basaran (2003), [31].

3. FINITE ELEMENT SIMULATION OF CONCURRENT LOADING ON A PRINTED CIRCUIT BOARD

In order to study the response under concurrent thermal and vibration loads using the constitutive model described above we have modeled an actual electronic package using the commercial finite element code ABAQUS where the constitutive model has been implemented by a user subroutine UMAT.. The studied assembly consists of a personal computer Printed Circuit Board (PCB) with the most relevant components mounted. The PCB is approximately 305mm long x 270mm wide with a thickness of 1.6mm and made of epoxy fiberglass known as FR-4. Properties for the materials other than solder joints are obtained from Pecht et al (1999), [32] and reported in Table 1. Pitarresi (2001), [33] performed dynamic testing and linear elastic finite element simulations of a similar PCB considering all the attached components. However the author did not consider the solder joints. In that study the natural frequencies and modal shapes of the PCB were measured and calculated with a 3D finite element model and the average stiffness and effective Young's modulus for different parts of the structure were measured. From the Pitarresi (2001), [33] analysis it is apparent that the fundamental mode of the structure induces flexure at the chipset and the processor locations. This is consistent with damage observed in the BGA solder joints during transportation. The corresponding finite element mesh is shown in Figure 1. In the first analysis set, we applied dynamic loading with amplitudes representative of those typically encountered during the service life, at 3 different frequencies and under isothermal conditions at room temperature. The dynamic loading was applied in the horizontal direction by imposing an acceleration history at the supported ends. A schematic of the applied dynamic load is shown in Figure 2. Second, we applied thermal loads only with the profile shown in Figure 3. In the final set of

analyses we applied the dynamic and thermal loads concurrently. The package was fully fixed at the ends, and the dynamic loading in form of input acceleration was prescribed at the support points and in the vertical direction. Modal analysis was performed first to determine the natural dynamic properties of the package. The first 5 modes are presented in Figure 4. Table 2 shows the first five natural frequencies of the structure. For the dynamical response an implicit direct integration scheme was used. The applied loads were harmonics with frequencies of 1Hz, 45Hz and 100Hz.

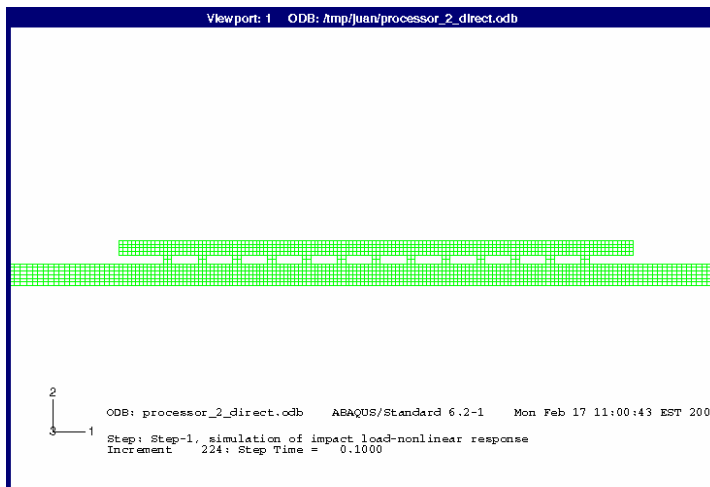
Tab.1 Material properties for the elastic components

| Material | E (GPa) | σ_y (MPa) | ν | ρ (tonne/mm ³) |
|-----------|---------|------------------|-------|---------------------------------|
| Pb37/Sn63 | 15.00 | 18.7 | 0.3 | 8.40E-09 |
| BT | 27.00 | ----- | 0.3 | 1.74E-09 |
| FR-4 | 20.30 | ----- | 0.3 | 4.07E-09 |
| UL 94V | 6.49 | ----- | 0.3 | 1.40E-09 |

Tab.2 Free vibration frequencies for the structure

| Mode | 1 | 2 | 3 | 4 | 5 |
|---------------------------|-------|--------|--------|--------|--------|
| Frequency(Hz) unloaded | 39.73 | 92.475 | 174.49 | 307.26 | 463.93 |

(a)



(b)

Fig.1 (a) Complete Finite Element Model. (b) Mesh at the chipset-PCB region.

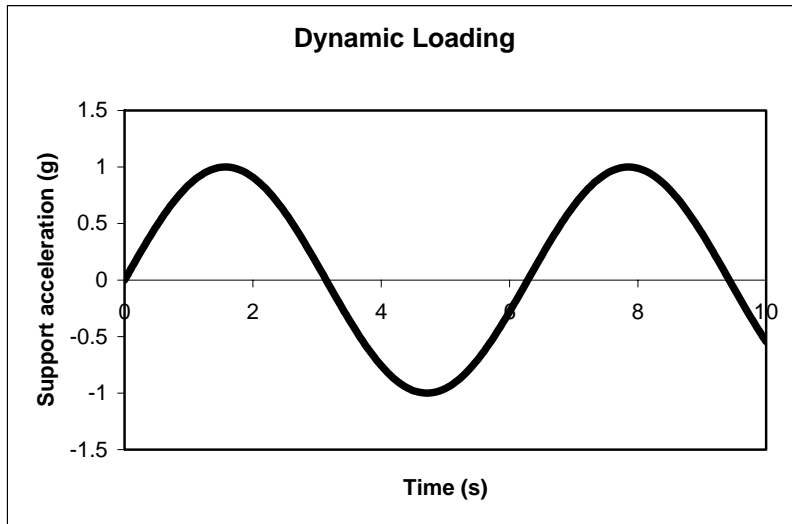


Fig.2 Schematic of the applied dynamic load.

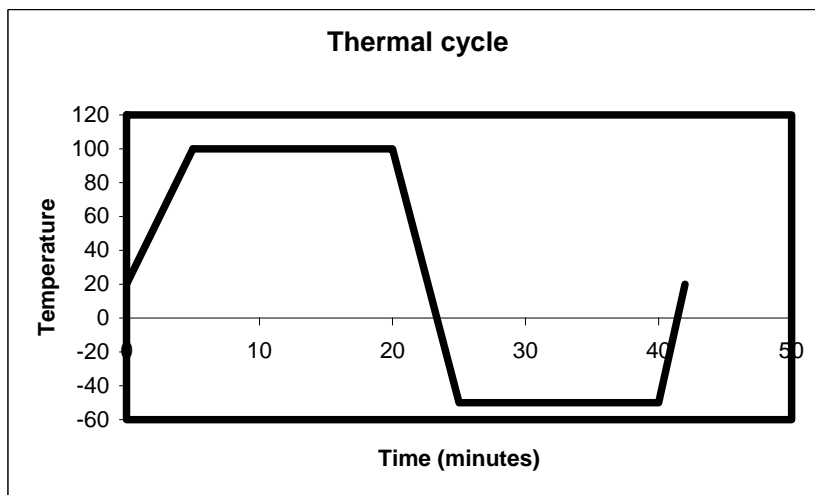


Fig.3 Schematic of the applied thermal profile.

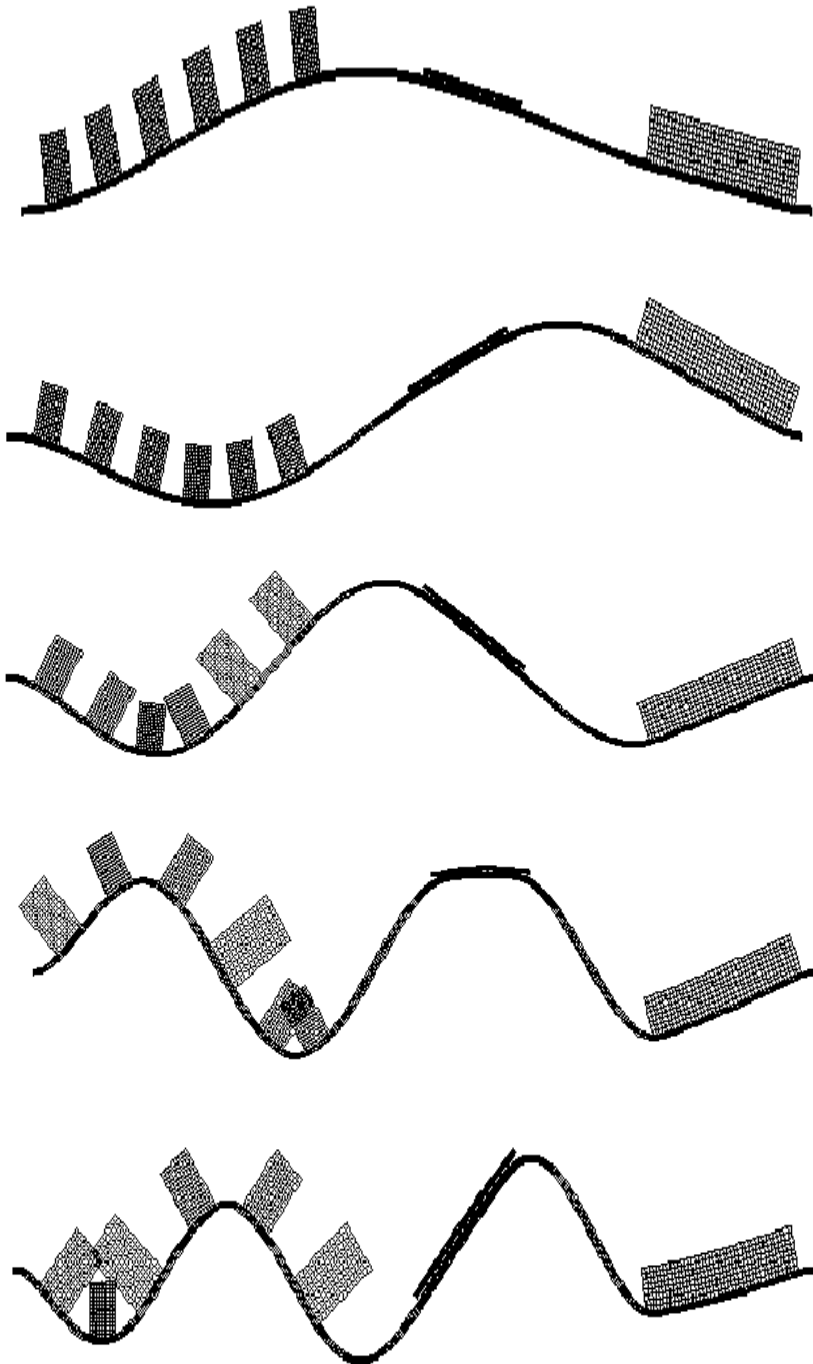


Fig.4 Modal shapes of the first 5 modes

4. RESULTS AND DISCUSSION

Figure 5 shows the relative displacement history at the center of the chipset for the studied frequencies. Figures 6a and 6b show the equivalent plastic strain induced by vibrations at 45Hz with two different time windows. The shown results are for the most-left solder joint in Figure 1b. At the 1Hz and 100Hz frequencies there is no vibration induced plastic strain. Figure 7 shows the history of Von Misses equivalent stress for all the frequencies and for the thermal loading case at the same solder joint. Clearly the thermal solution alone overwhelms the Misses stresses even for the near resonance frequency of 45Hz. The equivalent plastic strain for the same loading case as in Figure 7 is shown in Figure 8. There is plastic strain at the 45Hz vibration but is almost negligible as compared to the thermal solution. In order to evaluate the validity of Miners rule we added the contributions from the independent thermal and vibration analysis and labeled this result Miners in the subsequent plots. For the 1.0Hz frequency under dynamic loads alone there is no plastic strain and the Miners solution and thermal solutions are exactly the same. Comparison with the concurrent solution at 1.0Hz is shown in Figure 9. The applied dynamic loading at this particular frequency caused no plastic strain, however it did increase the damage when applied concurrently with the thermal loading. Furthermore the concurrent loading generates larger plastic strains as compared to the thermal loading case. This result suggests that although the trend behind Miners rule is in the right direction (i.e., damage increases) the effect of the concurrent loading considerable increases damage and a linear superposition of both effects is inaccurate. Figure 10(a) and 10(b) present similar results for the 45Hz frequency for the equivalent plastic strain and Von Misses equivalent stress. In Figure 11 the case of 100Hz frequency is included in the results. Our results show that when the plastic strains due to independently applied vibrational and thermal loads are linearly added together to avoid the concurrent loading analysis the prediction underestimates the concurrent loading response. Therefore, from the computational results it can be concluded that using Miners rule leads to much smaller equivalent plastic strain and Misses stress values as compared to the concurrent application of the thermal and vibration loads.

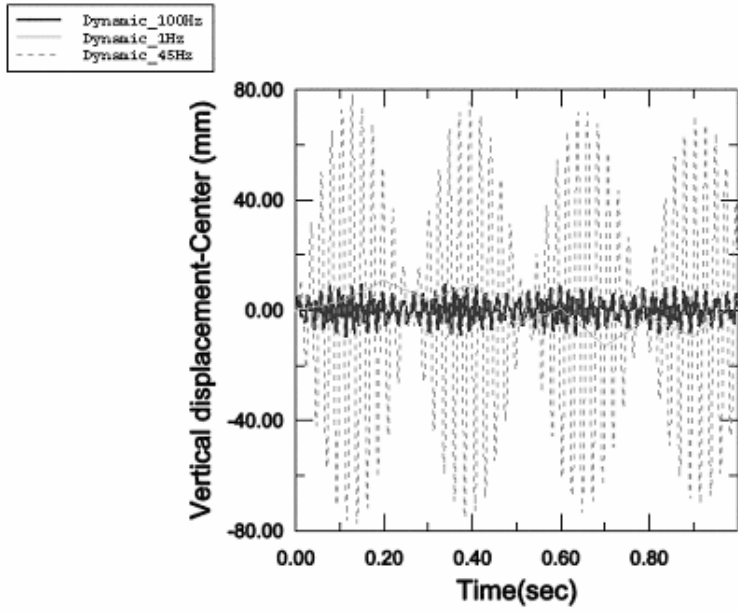
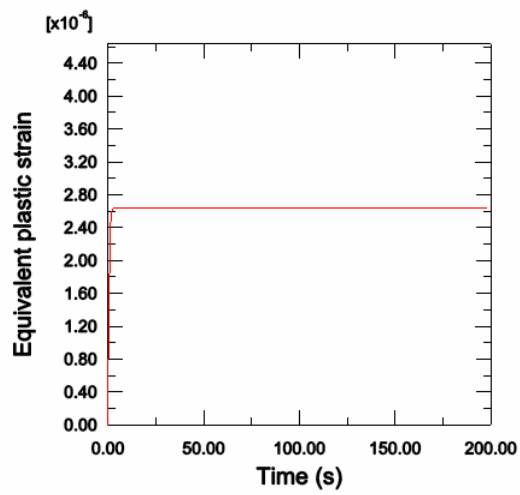


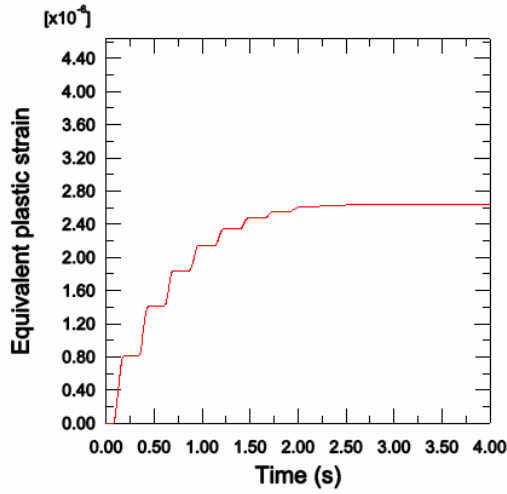
Fig.5 1Hz, 45Hz, 100 Hz –Dynamic loading only relative displacement.

SDV9 E: 10 IP: 4 ELSET SOLDER



(a)

SDV9 E: 10 IP: 4 ELSET SOLDER



(b)

Fig. 6 (a) 45Hz, Dynamic loading only equivalent plastic strain.
 (b) 45Hz, Dynamic loading only equivalent plastic strain.

MISES_100Hz
 MISES_1Hz
 MISES_45Hz
 MISES_THERMAL

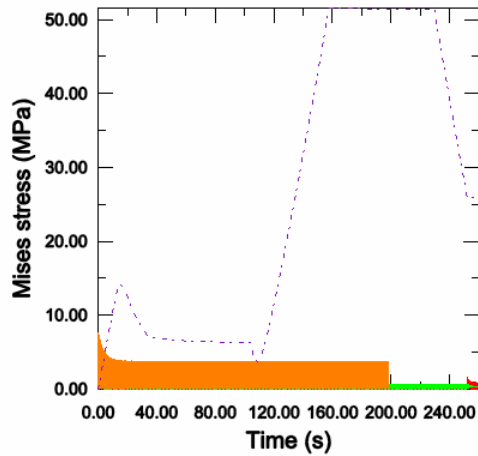


Fig.7 1Hz, 45Hz, 100Hz –Dynamic and thermal-Misses Stress

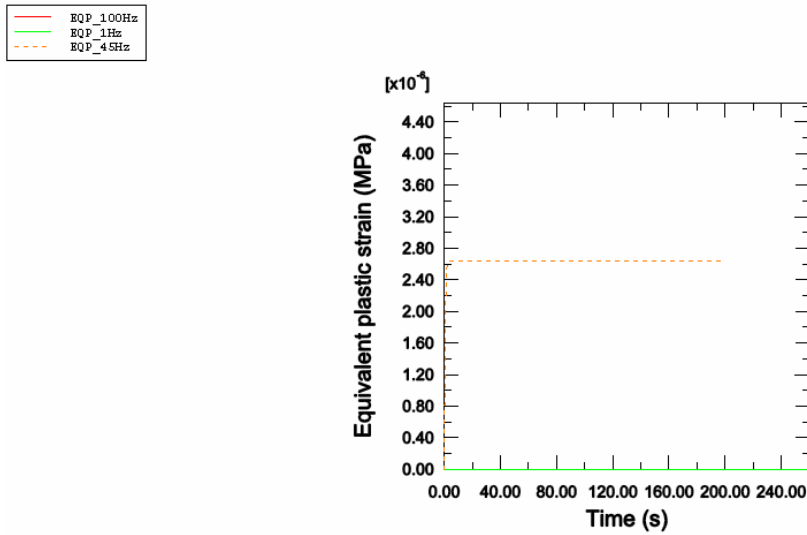


Fig.8 1Hz, 45Hz, 100Hz dynamic and thermal-Equivalent plastic strain.

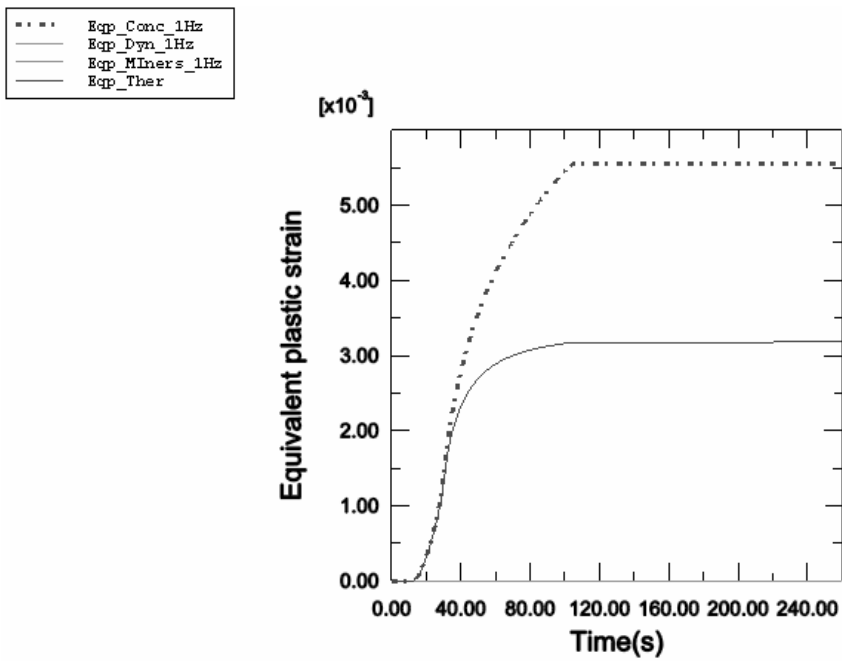
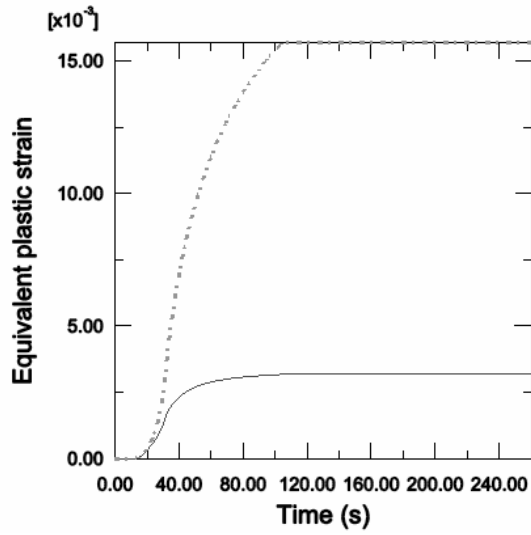
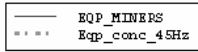
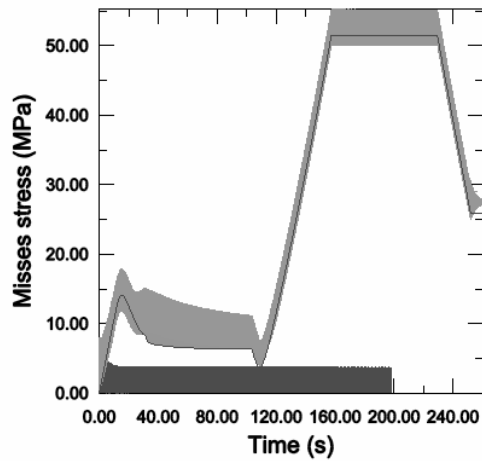
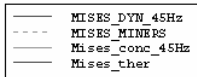


Fig.9 Equivalent plastic strain for the 1Hz Dynamic+thermal (Miners), concurrent and thermal load cases.



(a)



(b)

Fig.10 (a) Equivalent plastic strain for the 45Hz dynamic+thermal (Miners) and concurrent load cases. (b) Mises equivalent stress for the 45Hz dynamic+thermal (Miners) and concurrent load cases.

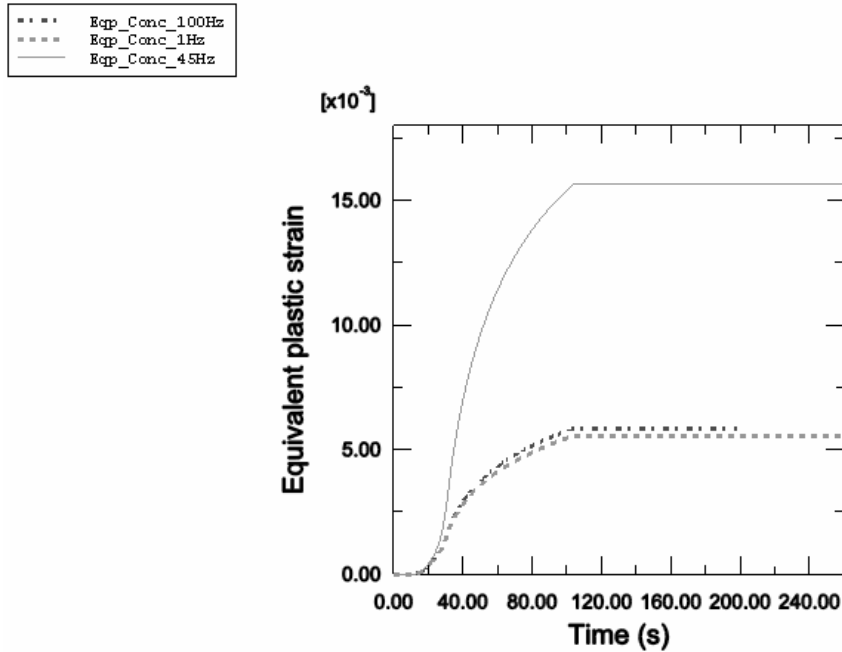


Fig.11 Equivalent plastic strain for the 1.0, 45.0 and 100Hz concurrent load case.

5. CONCLUSIONS AND RECOMMENDATIONS

A damage mechanics coupled elasto-viscoplastic constitutive model is proposed for analysis of microelectronic packaging under concurrent thermal and vibration loads. We have performed finite element analysis of electronic packaging under dynamic, thermal and concurrent (dynamic and thermal) load cases using a thermodynamics damage mechanics based rate dependent constitutive model for Pb/Sn solder alloys. The results from the simulations show that the superposition principle behind Miners rule that adds up the independent solutions from dynamic and thermal analysis to obtain the concurrent solution is correct for the boundary conditions and loading directions applied here. Yet, Miner's rule consistently underestimates the response of the system. The finite element simulations study conducted in here show that, using Miner's rule can lead to non-conservative results for certain boundary conditions and loading directions.

ACKNOWLEDGMENTS

This research project is supported by the United States Navy Office of Naval Research Advanced Electrical Power Systems Program, under the direction of director Terry Ericson.

REFERENCES

- [1]. Kitano, B. P., Kawai, S. and Shimizu, L, Thermal Fatigue Strength Estimation of Solder Joints of Surface Mount IC Packages, *Proc. 8th Annual Int. Elec. Packaging Conf., IEPS*, Dallas, Texas, pp.4-8, 1988.
- [2]. Lau, J. and Rice, J. R, Thermal Stress/ Strain Analyses of Ceramic Quad Flat Pack Packages and Interconnects, *Elect. Components and Technology 40th Conf.*, Vol.1, Los Vegas, Nevada, pp. 824-934, 1990.
- [3]. Basaran, C., Chandaroy R. and Zhao, Y, *Influence of Grain Size and Microstructure on Dynamic Response of Solder Joints*, 98-WA/EEP-12, ASME Publications.
- [4]. Adams, P. J. *Thermal Fatigue of Solder Joints in Micro-Electronic Devices*. M.S. thesis, Department of Mechanical Engineering, MIT, Cambridge, MA, 1986.
- [5]. Wilcox, J. R., Subrahmanyam, R., and Li, C. Thermal Stress Cycles and Inelastic Deformation in Solder Joints. *Proc. 2nd ASME Int. Electronic Mat. and Processing Congr.*, Philadelphia, PA, pp 208-211.
- [6]. Knoch, S. and Fox. L. R. Constitutive Relation and Creep-Fatigue Life Model for Eutectic Tin-Lead Solder. *IEEE Trans Comp. Hybrids Manuf. Technol*, 13 (1990).424-43.
- [7]. Darveaux, R. and Banerji, K. Constitutive Relations for Tin-Based Solder Joints. *IEEE Trans. Comp. Hybrids Manuf. Technol*, 15(1992)1013-1024.
- [8]. Hong, B. Z. and Burrell, L. G. Nonlinear Finite Element Simulation of Thermoviscoplastic Deformation of C4 Solder Joints in High Density Packaging Under Thermal Cycling. *IEEE Trans. Components, Packaging, and Manufacturing Technology-Part A*, 18(1995) 585-590.
- [9]. McDowell, D. L., Miller, M. P., and Brooks, D. C. A Unified Creep-Plasticity Theory for Solder Alloys. *Fatigue Testing of Electronic Materials, ASTM STP*, 1153 (1994)42-59.
- [10]. Zhao, Y.. Thermomechanical Behavior of Ball Grid Array Solder Joints Under Thermal and Vibration Loading; Testing and Modeling. *PhD Dissertation. University at Buffalo. The State University of New York*, 2000.
- [11]. Basaran, C., and Tang, H., Implementation of a thermodynamic framework for damage mechanics of solder interconnect in microelectronic packaging. *Proceedings of IMECE, 2002 ASME International Mechanical Engineering Congress & Exposition., New Orleans, Louisiana*.
- [12]. Tang, H. A Thermodynamic Damage Mechanics Theory and Experimental Verification for Thermomechanical Fatigue Life Prediction of Microelectronics Solder Joints. *PhD Dissertation. University at Buffalo. The State University of New York*. 2002
- [13]. Kashyap, B., and Murty, G.. Experimental Constitutive Relations for the High Temperature Deformation of a Pb-Sn Eutectic Alloy. *Mater.Sci. and Engin*, 50(1981) 205-213.
- [14]. Gomez, J., and Basaran, C. Determination Of The Strain Gradient Plasticity Length Scale For Microelectronics Solder Alloys. *Submitted to Inter. J. Plasticity*.
- [15]. Gomez, J., and Basaran, C. Nanoindentation of Pb/Sn Solder Alloys;Experimental and Finite Element Simulation Results. *Inter. J. Solids and Struc. in press*
- [16]. Steinberg, D.S. Vibration Analysis for Electronic Equipment. *2nd Edition., John Wiley & Sons, New York*. (1988)
- [17]. Basaran, C., Zhao, Y., Tang, H., and Gomez, J. A Damage Mechanics Based Constitutive Model for Joints. *ASME J. Electronic Packaging*, 127 (2005) 1-7.
- [18]. Simo, J., and Hughes, T. Computational Inelasticity. *Interdisciplinary applied mathematics. Springer*. 1998
- [19]. Owen, D.R.J. and Hinton, E.. *Finite Element in Plasticity*, Pineridge Press Limited, Swansea, U.K. 1980.
- [20]. Zhao, Y., Basaran, C., Cartwright, A., and Dishongh, T. Thermomechanical Behavior of Micron Scale Solder Joints: An Experimental Observation. *J. Mech. Behavior of Mater*, 10(1999)135-146.
- [21]. Barker, D., Vodzak, J., Dashgupta, A., and Pecht, M. Combined Vibrational and Thermal Solder Joint Fatigue. A Generalized Strain versus Life Approach. *ASME J. Elec. Packaging*, 2(1990) 129-134.
- [22]. Miner, M.A. Cumulative Damage in Fatigue. *ASME J. Applied Mech.* 1945
- [23]. Lubarda, V and Benson, D.. On the numerical algorithm for isotropic-kinematic hardening with the Armstrong-Frederick evolution of the back stress. *Comput. Methods Appl. Mech. Engrg*, 191(2002)3583-3596.

- [24]. Alfano, G., De Angelis, F., and Rosati, L. General Solution Procedures in Elasto/Viscoplasticity. *Comput. Meth. Appl. Mech. Eng.*, 190(2001) 5123-5147.
- [25]. Chaboche, J. Constitutive equations for cyclic plasticity and viscoplasticity. *Inter. J. Plasticity*, 3(1989) 247-302.
- [26]. Armstrong, P. J., and Frederick, C. O. A Mathematical Representation of the Multiaxial Bauschinger Effect. *CEGB Report RD/B/N731*. 1996
- [27]. Prager, W. A new method of analyzing stress and strains in work-hardening plastic solids. *Journal of Applied Mechanics*, 23 (1956) 493-496.
- [28]. Lemaitre, J. *A course on damage mechanics*. Springer-Verlag. Germany. 1996
- [29]. Basaran, C., and Yan, C. A Thermodynamic Framework for Damage Mechanics of Solder Joints. *Journal of Electronic Packaing, Trans. ASME*, 120(1998) 379-384.
- [30]. Basaran, C., and Nie, S. An Irreversible Thermodynamic Theory for Damage Mechanics of Solids. *International Journal of Damage Mechanics*, 13(2004) 205-224.
- [31]. Gomez, J and Basaran, C. Numerical Simulation of Monotonic and Fatigue Shear Testing of Thin Layer Solder Joints Using a Damage mechanics Based Constitutive Model. *Proceedings 2003 ASME Mechanics and Materials Conference, Scottsdale, Arizona*.
- [32]. Pecht, M., Agarwal, R., Mc Cluskey, P., Dishong, T., Javadpour, S. and Mohajan, R. *Electronic packaging materials and their properties*. CRC press. 1999.
- [33]. Pitarresi, M. Estimating Shock and Vibration Response in Personal Computers. *Yearly Report. Department of Mechanical Engineering, State University of New York at Binghamton, December*. 2001.